Journal of Materials Research and Technology 27 (2023) 6344–6357

Contents lists available at ScienceDirect

Journal of Materials Research and Technology

journal homepage: www.elsevier.com/locate/jmrt

Nanocrystalline cellulose from lactic acid hydrolysis of pepper waste (*Piper nigrum* L.): Response surface methodology optimization and application in bio-composite

Holilah Holilah [a,b,**], Lisman Suryanegara [a,b], Hasliza Bahruji [c], Nanang Masruchin [a,d], Suprapto Suprapto [e], Ratna Ediati [e], Asranudin Asranudin [f], Aishah A. Jalil [g,h], Dini Viandi Ramadhani [i], Zuratul Ain Abdul Hamid [j], Didik Prasetyoko [e,*]

[a] Research Center or Biomass and Bioproducts, National Research and Innovation Agency of Indonesia (BRIN), Cibinong, 16911, Indonesia
[b] Research Collaboration Center for Nanocellulose, BRIN-Andalas University, Padang, 25163, Indonesia
[c] Centre of Advanced Material and Energy Sciences, Universiti Brunei Darussalam, Jl. Tungku Link, BE 1410, Brunei
[d] Research Collaboration Center for Biomass and Biorefinery Between BRIN and Universitas Padjadjaran, Jatinangor, 45363, Indonesia
[e] Department of Chemistry, Faculty of Science and Data Analytics, Institut Teknologi Sepuluh Nopember, Surabaya, Indonesia
[f] Department of Food Science and Technology, Halu Oleo University, Kendari, Indonesia
[g] Centre of Hydrogen Energy, Institute of Future Energy, Universiti Teknologi Malaysia, 81310 UTM Johor Bahru, Skudai, Johor, Malaysia
[h] Department of Chemical Engineering, Faculty of Chemical and Energy Engineering, Universiti Teknologi Malaysia, 81310 UTM Johor Bahru, Skudai, Johor, Malaysia
[i] Department of Biology, Faculty of Science and Data Analytics, Institut Teknologi Sepuluh Nopember, Surabaya, Indonesia
[j] School of Materials & Mineral Resources Engineering, Universiti Sains Malaysia, 14300 Nibong Tebal, Pulau Pinang, Malaysia

ARTICLE INFO

Handling Editor: SN Monteiro

Keywords:
Nanocrystalline cellulose
Lactic acid
Optimization
Bio-composite

ABSTRACT

Nanocrystalline cellulose (NCs) was successfully isolated from pepper biowaste using lactic acid hydrolysis and employed as filler in seaweed biocomposite. Optimization of hydrolysis parameters by employing response surface methodology (RSM) generates 75.50 % NCs with 76.68 % crystallinity at 6.31 M lactic acid, 3.02 h and 85.86 °C. The ANOVA analysis indicates hydrolysis efficiency requires precise temperature control and lactic acid concentration to obtain high crystalline cellulose at high production yield. The NCs displayed rod-shaped morphology with 29.65 ± 3 nm diameter and 335.19 ± 10 nm length, with a negative zeta potential and higher thermal stability than the cellulose. NCs addition as filler in seaweed biofilm improved the tensile strength but reduced the elongation at break. The biofilm exhibits excellent properties in reducing water adsorption, solubility, and water permeability by increasing nanocellulose filler.

1. Introduction

Nanocrystalline cellulose (NCs) is an increasingly important green material for broad industrial applications due to its excellent chemical, optical and mechanical properties [1–5]. As a biodegradable material with lightweight and high mechanical properties, NCs were employed as fillers to improve the tensile strength and stiffness of biopolymer [6]. The nanosize will improve the dispersion and integration in the polymer matrix, while the crystallinity of cellulose is essential in improving thermal stability, mechanical strength, and gas permeability. Isolation of NCs from lignocellulosic biomass requires alkalization and bleaching processes to remove lignin and hemicellulose, followed by acid hydrolysis. Hydrolysis of cellulose into NCs relies on the dissolution of polymeric cellulose into sugar monomer. The hydrolysis time, temperature, acid concentration, and acid strength affect crystallinity and the yield of nanocellulose [7]. Hydrolysis using strong acid causes second-stage hydrolysis, particularly at high temperatures [8]. The microfibril cellulose dissolved into sugar in the second hydrolysis stage, decreasing the nanocellulose yield and crystallinity [9].

As an alternative to corrosive inorganic acid, organic acid was used to produce NCs with high thermal stability and yield [10]. Organic acid maintains the crystal structure of cellulose, producing nanocellulose with high thermal stability [11,12]. Hydrolysis of disposable paper glass using citric acid produced a 65 % yield of rod-like shaped NCs at 94.2 %

* Corresponding author. Department of Chemistry, Faculty of Science and Data Analytics, Institut Teknologi Sepuluh Nopember, Surabaya, 60111, Indonesia.
** Corresponding author. Research Center or Biomass and Bioproducts, National Research and Innovation Agency of Indonesia (BRIN), Cibinong, 16911, Indonesia.
E-mail addresses: holi003@brin.go.id (H. Holilah), didikp@chem.its.ac.id (D. Prasetyoko).

https://doi.org/10.1016/j.jmrt.2023.11.084
Received 13 July 2023; Received in revised form 31 October 2023; Accepted 9 November 2023
Available online 15 November 2023

crystallinity [12]. Oxalic acid and formic acid were also reported to produce NCs with high crystallinity and yield at 60–94 % [13–17]. Lactic acid is another potential organic acid for hydrolysis that can reduce the environmental effect of inorganic acids. Lactic acid is produced from the fermentation of molasses using Lactobacillus sp., mainly used in the food industry [18]. Lactic acid ionization produces lactate and H^+ ions, with pKa approximately similar to formic acid at 3.86. In acid hydrolysis, easy diffusion of H^+ into the cellulose network and the ability of the counter anion to disrupt massive hydrogen bonds are essential to enhance the hydrolysis rate [19]. Therefore, optimization of the acid concentration, hydrolysis time and reaction temperature are necessary to improve acid diffusion through the robust crystal structure of a highly stable natural cellulose.

Choosing the right experimental design is essential when several variables determine a group of responses. The Response Surface Methodology (RSM) has been employed to optimize the outcomes of various hydrolysis parameters [20–22]. Quadratic response surfaces such as the Box-Behnken design (BBD), a three-level factorial, identify the ideal conditions for NCs isolation from microcrystalline cellulose [23], tea-stalk cellulose [24], bamboo shoots and kenaf plants [22,25]. Indonesia produced 90,000 tons of pepper in 2019 (Direktorat Jenderal Perkebunan Indonesia), with approximately 80 % of the harvested fruits discarded as biowaste. The pepper stalk (PW) contained 77.9 % cellulose, suitable for conversion into nanocellulose [26]. The isolated NCs is used as filler in seaweed biofilm to improve the mechanical properties, morphology, water adsorption capacity, solubility, and water vapor permeability. NCs were employed as fillers to improve tensile strength and stiffness of biopolymer [27–30]. The hydroxyl groups in the NCs formed strong interfacial interactions through hydrogen or ionic bonds with the polymer matrix, reducing the freely available hydroxyl group [31]. This causes a decrease in film hydrophilicity, water permeability and solubility [28,32–35]. Therefore, optimization of lactic acid concentration, hydrolysis temperature, and time is important to improve the effectiveness of NCs as fillers. This study uses the BBD to obtain a high yield and crystallinity nanocellulose from microcrystalline cellulose isolated from pepper biowaste. Statistical analysis using analysis of variance (ANOVA) provides insight into the main hydrolysis parameters affecting NCs formation.

2. Materials and method

The cellulose used in this study was obtained using the method reported in previous work [26]. Pepper stalk waste (PW) was obtained from the pepper industry, Kendari, Indonesia. The Lactic acid ($CH_3CH(OH)COOH$) and sodium hydroxide (NaOH, ≥99 %) were obtained from Sigma Aldrich, Singapore. Hydrogen peroxide (H_2O_2, 30 % (w/w) in H_2O and Glycerol, 85 % were bought from Merck, Germany. Seaweed from *Eucheuma cottoni* (moisture content <2 %) was supplied from the Food Processing and Chemical Analysis Laboratory, Department of Food Science and Technology, Halu Oleo University, Indonesia.

2.1. Isolation of cellulose from PW

Obtained from the stalk, a PW of 500 g was soaked in water at 80 °C for 4 h to initialize the isolation of cellulose from the stalk. The stalk was ground into powder after drying at 100 °C. The powder obtained was mixed at a weight-to-volume ratio of 1:20 with a 5 % NaOH solution. The combination underwent filtering and deionized water washings to achieve pH neutrality. A mixture of 3 % (v/v) H_2O_2 and 5 % NaOH solution was used to bleach the powder, with a waste-to-reagent ratio of 1:40 (w/v). Vacuum filtration was used to separate the mixture after it had been agitated at 55 °C for 90 min. Deionized water was used to wash away the powder residue until the pH of the supernatant was neutral. The final process step was re-alkalization. The technique used for alkalization was similar to that applied for re-alkalization, with hydrothermal replacing the traditional thermal procedure [26]. The hydrothermal process produced a solid residue, which was filtered, cleaned, and dried at 60 °C. The final product is known as cellulose from PW sample (PW–C).

Table 1
The range of the parameters of the design matrix.

Parameter	Unit	Low-level Xi = −1	Midrange level Xi = 0	High level Xi = 1
X_1 LA concentration (A)	M	5	6	7
X_2 Hydrolysis time (B)	h	2	4	6
X_3 Temperature (C)	°C	60	80	100

2.2. Preparation of nanocellulose using lactic acid hydrolysis

Cellulose from pepper waste (PW–C) was subsequently hydrolyzed using lactic acid. The ratio of solid to liquid was 1:50, and the hydrolysis condition was summarized in Table 1. After hydrolysis, the nanocellulose suspension was ultrasonicated using BioBase Ultrasonic Cell Disruptor UCD-1200 for 15 min. After this process, the nanocellulose suspension was rinsed using deionized water by centrifugation and then dialyzed against distilled water using cellulose tubing membranes (12–14 kDa molecular weight cut-off) for three days to achieve a pH of 6.5–7. The sample obtained was denoted as PW-NCLA.

2.3. Design of experiment

RSM design of experiments has been demonstrated to be an effective tool for analyzing various experimental conditions. This statistical method applies a polynomial equation to experimental data, accurately describing a data set's response. The RSM using BBD model was used to optimize and find the best-operating conditions for the hydrolysis of PW-C cellulose. Acid concentration, temperature, and hydrolysis time were varied to obtain optimum hydrolysis conditions, with the yield and crystallinity as the responses. The polynomial equation below was used to calculate the number of experiments required for BBD. Table 1 shows the range of parameters tested with various coding levels.

$$Y = b_o + b_1A + b_2A + \ldots + b_1A^2 + b_2B^2 \ldots + b_{12}AB + b_{13}AC \ldots + \varepsilon \ldots\ldots\ldots \quad (1)$$

where Y represents the response, *bo* is the offset term, *b1*, *b2*, and *b12* are the factor coefficients, A, B, and C are the model's independent variables, ε is the statistical error and A^2, and B^2 are the interaction parameters.

2.4. Functional group analysis

The functional group of materials was observed using Fourier transform infrared spectroscopy (FTIR, Shimadzu Instrument Spectrum One 8400S). Powdered nanocellulose (1 mg) was mixed with KBr (99 mg) and pressed into pellets. The FTIR spectra of the samples were monitored in the range of 400–4000 cm^{-1}.

2.5. Crystallinity analysis

The phase and crystallinity of nanocellulose were determined using X-ray diffraction (XRD, PHILIPS-binary Xpert). The samples were analyzed with Cu Kα radiation = 1.54056 Å as X-ray source, at 40 kV and 30 mA. The crystallinity index (CI) of NCs was estimated using the equation below.

$$CI(\%) = [(I_{002} - I_{am}) / I_{002}] \times 100 \ldots\ldots\ldots \quad (2)$$

where I_{002} was intensity of the [002] lattice diffraction line at around 2θ

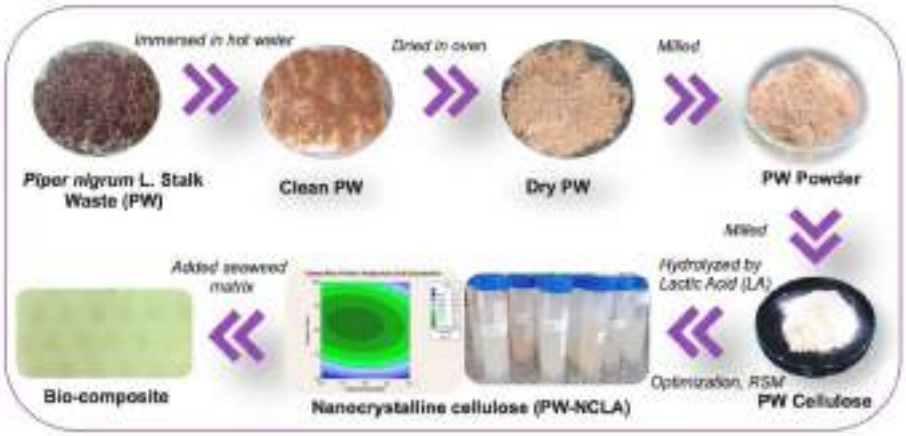

Fig. 1. The schematic diagram of pepper waste conversion to nanocrystalline cellulose/seeweed bio-composite.

= 22–23°, and I_{am} was intensity of the amorphous region's at around 2θ = 18–19°.

2.6. Morphological and particle size analysis

The structure, shape, and size of nanocellulose from PW-C cellulose were examined using Transmission Electron Microscopy (TEM, Hitachi HT-7700). Nanocellulose was dispersed in distilled water at 1 wt%/vol. and sprayed on the copper grid's surface. The samples were examined after water had evaporated at about 25 °C. The width of the length of nanocellulose was calculated using Image-J software. Apart from that, the morphology of waste and cellulose of PW were examined using scanning electron microscopy (SEM, Hitachi Flex SEM 100).

2.7. Particle size and zeta potential analysis

The particle size and zeta potential of nanocellulose were analyzed using Malvern Particle Size Analyzer. The nanocellulose sample was placed in the cuvette after being suspended in distilled water. The materials were examined using dynamic light scattering and a particle size analyzer. The measurements were taken three times at room temperature, in the 0.1–10.000 nm region. The data was processed using Delsa Nano Software.

2.8. Thermal analysis

The Hitachi High-Tech Sciences STA7200 Simultaneous Thermal was used to assess the thermal decomposition behavior of NCs. The samples were placed in an alumina crucible, and the thermal decomposition was carried out from 28 °C to 600 °C at a rate of 10 °C/min under an N_2 environment.

2.9. Preparation of bio-composite

The bio-composite was prepared using a seaweed matrix. The nanocellulose was used as filler at 1, 3, 5 and 7 % loading to the matrix. PW-NCLA was dispersed in distilled water, stirred for 1 h, and then sonicated for 30 min (Qsonica Sonicator Q500, USA). On the other hand, 2 g of seaweed was mixed with 50 mL of distilled water. Nanocellulose was added slowly to the seaweed solution. Then, 3 % glycerol was added and stirred at 80 °C for 20 min 50 mL of film suspension was poured onto a casting plate and dried at room temperature for 48 h. After drying, the bio-composite film layer was removed from the mold. A control bio-composite film was also produced using glycerol and seaweed but without nanocellulose filler. The seaweed films with 1, 3, 5 and 7 % PW-NCLA were denoted as Se–1NC, Se–3NC, Se–5NC and Se–7NC, respectively. The film without nanocellulose filler was marked as Se. Fig. 1 summarizes the schematic diagram of pepper waste transformation to nanocrystalline cellulose/seaweed bio-composite.

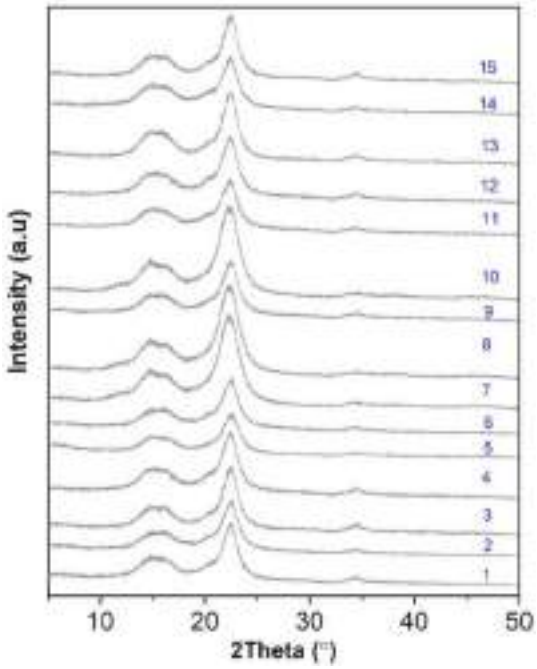

Fig. 2. XRD pattern of the samples isolated with different combinations of acid concentration, hydrolysis time, and temperature.

2.9.1. Characterization of seaweed filled nanocellulose bio-composite

The mechanical properties of the bio-composite film were evaluated using universal testing machine (Strograph VG 10-E) at room temperature with 10 kN load according to ASTM D-882-91. The morphological analysis of the surface and cross-section of the film was characterized by a Hitachi Flex SEM 100. The water adsorption, solubility, and water permeability of seaweed-NC film were also measured. The water adsorption was analyzed through reduction of the initial film weight and after drying [36]. The solubility of film was determined according to the method reported by Ref. [37]. The solubility percentage of the film is the percentage of the film dissolved in water after 24 h of immersion. Water vapor permeability was tested using the ASTM gravimetric method (1995). The film was stretched over a circular permeation cell tube with a diameter of 4 cm. Inside the permeation cell put silica gel (0 % RH). After being covered with a film, the permeation cell was placed in a

Table 2
NCs yields and crystallinity under different parameters in the experimental design.

X1 (LA concentration(M))	X2 (Hydrolysis time (h))	X3 (Temperature (°C))	Yield		Crystallinity Index (CI)	
			Observed	Predicted	Observed	Predicted
5	4	60	59.08	58.86	66.32	66.24
5	2	80	63.13	63.32	59.90	59.56
5	6	80	69.83	69.98	73.75	72.01
5	2	100	68.01	67.86	70.21	70.46
7	6	80	61.25	61.05	54.19	54.52
6	6	100	63.34	63.32	56.08	56.59
6	4	80	75.80	75.97	77.68	77.75
6	4	80	75.24	75.97	77.83	77.75
6	2	100	57.57	57.64	63.92	63.16
6	4	80	76.89	75.97	77.76	77.75
7	4	100	61.71	61.92	63.97	63.12
7	2	80	68.03	67.87	70.50	71.27
7	4	60	60.27	60.41	72.26	72.00
6	2	60	52.65	52.31	63.68	63.17
6	2	60	58.14	58.15	69.57	70.41

desiccator filled with saturated NaCl solution (70 % RH) at 30 °C. The water vapor transmission rate (WVTR) can be determined from the weight of the permeation cell. The film thickness was also measured using a micrometer.

3. Results and discussion

3.1. Optimization of nanocellulose isolation

Hydrolysis was optimized using three independent variables, i.e., lactic acid concentration, temperature, and hydrolysis time. Each factor consists of 3 levels of variation at 5, 6, and 7 M of lactic acid concentration, at 60, 80, and 100 °C temperature, and at 1, 3, and 5 hydrolysis hours. The optimization parameter employed the Box Behnken Design model with 15 experimental sets and the response to yield and crystallinity. The XRD analysis of the nanocrystalline cellulose from different hydrolysis parameters was used to determine the crystallinity index of nanocrystalline cellulose (Fig. 2). The yield and the crystallinity index, CI are summarized in Table 2.

Contour plots and three-dimensional response surfaces depict the combined effect of the two factors on the response while the other factor remains constant. Fig. 3a demonstrates the interaction between the reaction temperature and the lactic acid concentration on NCs yield at 3 h. Increasing the temperature from 60 °C to 80 °C enhanced the NCs yield. High temperature improves the mass transfer of lactic acid into the intraparticle cellulose pores, leading to efficient hydrolysis. However, hydrolysis at high lactic acid concentration harms the nanocellulose yield. An elliptical contour plot showed a significant interaction between temperature and acid concentration (Fig. 4a). A similar observation was found in the effects of the crystallinity. The crystallinity is enhanced at elevated temperatures due to the removal of amorphous cellulosic fragments and the rearrangement of microfibril to form a high-order crystalline structure. A high concentration of H^+ in the solution disintegrated the microfibril structure into the nanocrystal cellulose by removing the amorphous fragment. However, an optimum acid concentration must be employed to prevent the disintegration of crystalline fragments [38].

Figs. 3(b) and 4(b) show the effect of temperature and time while using 6 M lactic acid. The percentage yield and crystallinity increased when the reaction temperature and hydrolysis time were enhanced due to the increased diffusion of lactic acid into the amorphous cellulose fragments. However, further increasing the temperature and hydrolysis time was detrimental to the crystallinity as more surface area of cellulose was exposed for further reaction with acid, producing small particles with a low crystallinity index [23].

The effect of lactic acid concentration and time but at a constant reaction temperature of 80 °C is shown in Figs. 3(c) and 4(c). The results showed that increasing the concentration from 5 M to 7 M showed a volcano trend in the yield. High acid concentration causes the increase of cellulose swelling, which leads to the expansion of the surface area available for hydrolysis and dissolution into sugar monomers. The elliptical contour plot illustrates the significant interaction between acid concentration and hydrolysis time on the yield and crystallinity of cellulose [39].

3.1.1. Statistical analysis

The effect of hydrolysis parameters was determined using the Box Behnken Design. The responses of the 15 samples were based on a three-factorial design, as presented in Table 2. The results showed that the yield ranges from 52.65 % to 76.89 %, and the maximum yield was obtained at 6 M of acid concentration while hydrolyzed for 4 h at 80 °C. The NC crystallinity ranged from 54.19 % to 77.83 %, with the maximum crystallinity obtained when hydrolysis was conducted using 6 M lactic acid for 4 h and at 80 °C. Fig. 5 depicts a linear plot of the actual data versus the predicted data on the percentage yield and the crystallinity of NC. The predicted and experimental values were relatively close, and the high R^2 values were obtained at 0.9978 and 0.9956.

The results were further analyzed based on the ANOVA value to indicate the precision of the data. The fitness and significance of the model fitting are described using the F-value. The statistical significance is considered if the F-value is greater than the critical F-value at a level of 5 %. The F values on yield and crystallinity were determined at 249.52 and 124.75, respectively, indicating the high significance of the model. The higher F value indicates the accuracy of the model [23]. This statistical analysis determines the accuracy of the applied three-level factorial design model. In addition to the F value, the P value of the ANOVA evaluates the degree of significance of each variable examined in the hydrolysis of nanocellulose. The P value is significant if it is less than 0.05 [40]. The model has a significant P value of <0.0001 for yield and crystallinity responses (Table 3). As a result, the research above confirms that the response surface model is appropriate for optimizing the NCs extraction conditions in the current study. In addition, the P values for all the variables are less than 0.05, indicating a significant effect of the variables on the yield and crystallinity of PW-NCLA. The interaction of acid concentration and hydrolysis temperature significantly affected the yield and crystallinity of NCs PW. However, the single variable hydrolysis time showed no significant effect on the yield of nanocrystalline cellulose. The effect of hydrolysis time was only significant following the interaction with other variables such as acid concentration and hydrolysis temperature.

In addition to the F and P values, the R^2 value was also evaluated to determine the accuracy of the model. R^2 represents the strength of the interaction between independent variables that affect the value of the dependent variable and ranges from 0 to 1. The model accuracy issued

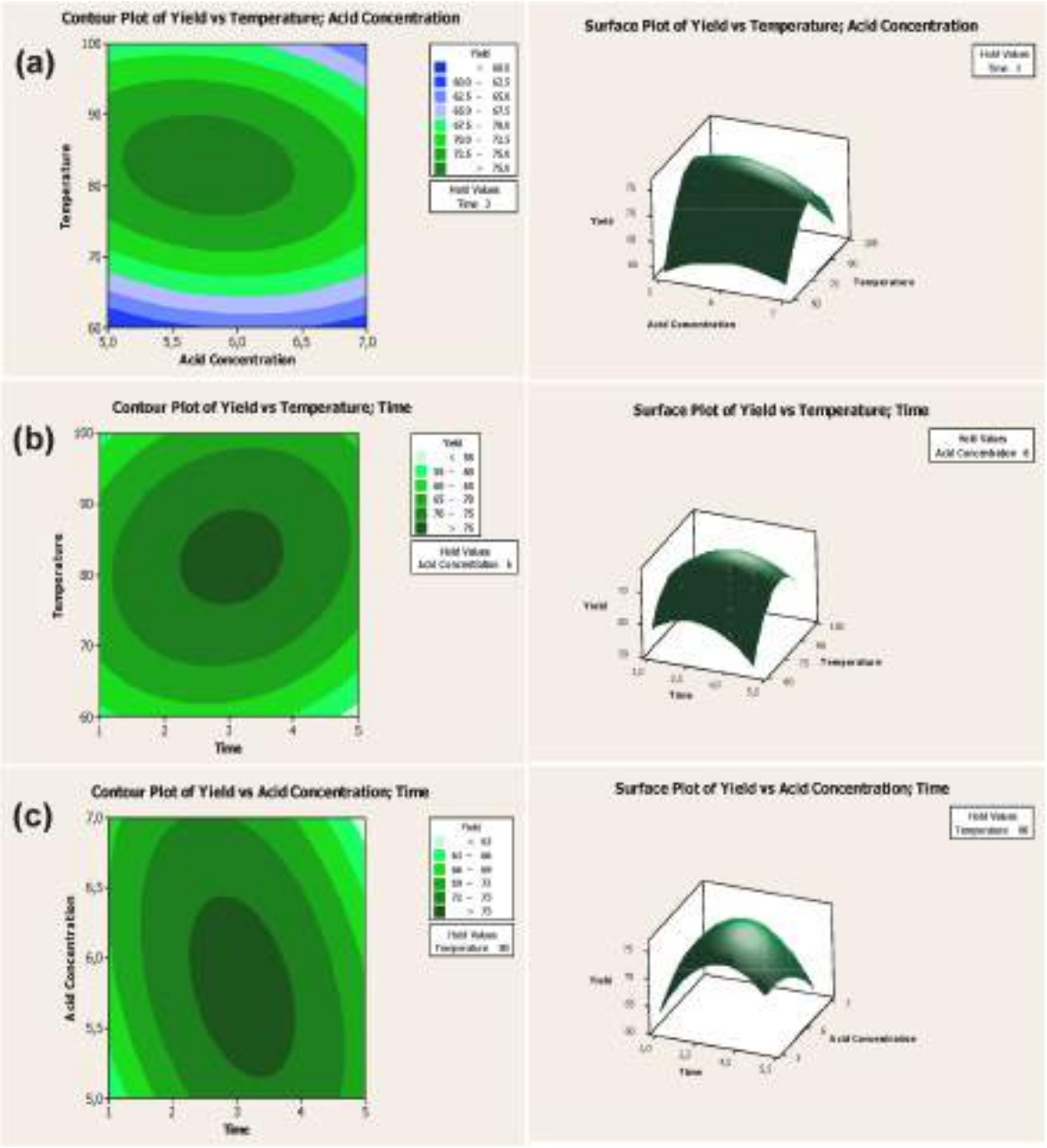

Fig. 3. Response surface plot for interaction between hydrolysis time, temperature, and concentration of acid on yield of nanocellulose.

by the regression R^2 is closer to one [41]. The R^2 value is one of the factors used to validate the model's response. The R^2 value must be more than 0.8 for the fit model, as a lower R^2 value indicates the model is unsuitable for explaining the relationship between variables [42]. However, a high R^2 value is not always a sign of a suitable model. Therefore, it is essential to determine the value of adj R^2 for the model, which provides a more precise evaluation of the adequacy of the model [42]. In adj-R^2, the value considered the number of data samples and the number of variables used in the experimental design. The results from ANOVA and regression showed that R^2 values were 0.9970 and 0.9930 for yield and crystallinity, respectively. In contrast, the value of adj R^2 obtained was 0.9950 and 0.9870 for yield and crystallinity, respectively. High values of R^2 and adj R^2 (respectively >0.9) indicate that the regression model shows a relationship between the response and the independent variable in the experimental range of variables. Moreover, the term 'lack of fit' denotes a model's failure. For the best model, besides the p-value of the model should be significant ($p < 0.05$), the p-value of lack of fit should be non-significant ($p > 0.05$). The p-value of lack of fit was non-significant for yield response namely 0.936.

3.1.2. *Validation of the model*

The optimization curve for the yield response and crystallinity of PW-NCLA are shown in Fig. 6(a) and (b). The optimization of the three independent variables on the response was evaluated through the composite desirability value. The yield response and crystallinity composite desirability values are 1 and 0.9999, respectively. A value equal to 1 indicates a very satisfactory solution, whereas a value of 0 denotes that the response fell outside of the acceptable range [25]. Based on the curve, the optimum condition to obtain a high NCs yield is at 6.31 M of lactic acid concentration, 3.02 h of hydrolysis time, and at 85.8 °C. Meanwhile, an optimum crystallinity of NCs is obtained at 5.20 M of lactic acid concentration, 3.67 h of hydrolysis time, and 82.62 °C. The

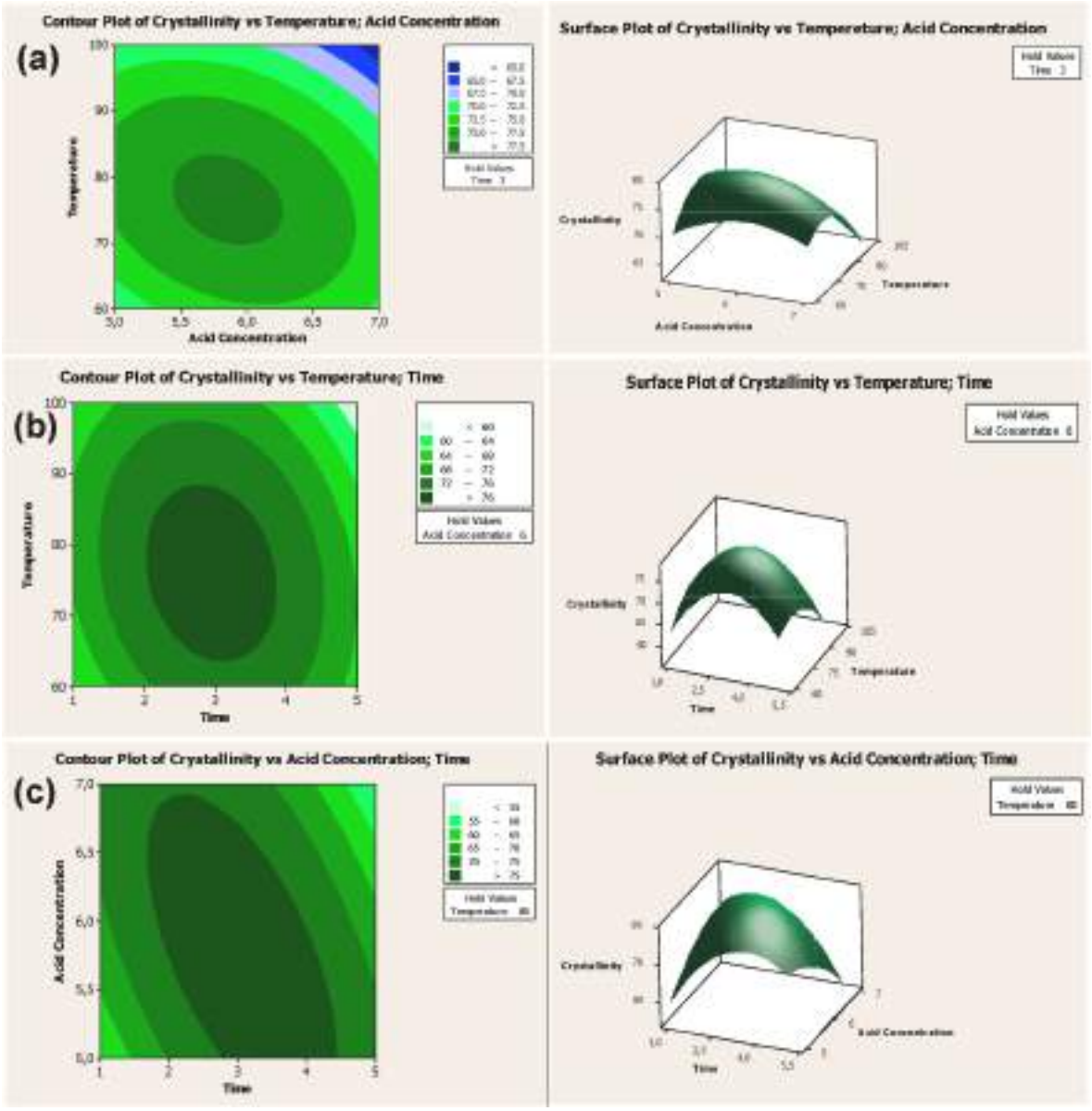

Fig. 4. Response surface plot for interaction between temperature, and concentration of acid on the crystallinity of nanocellulose.

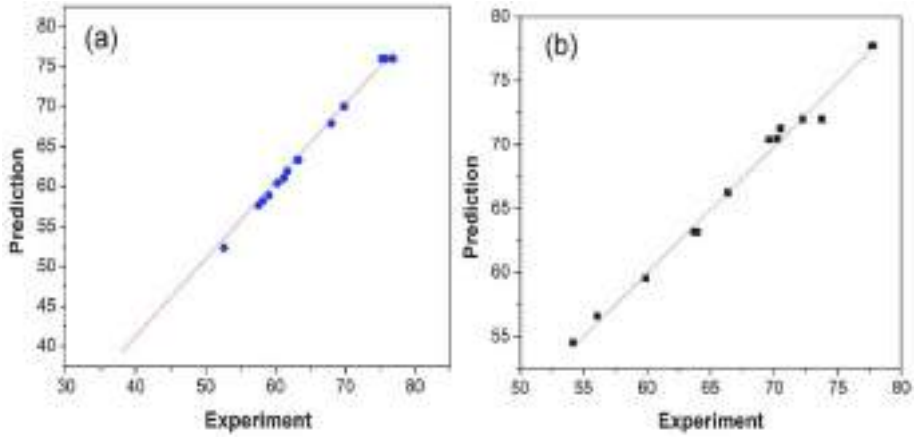

Fig. 5. Linear plot of actual versus predicted response of (a) yield and (b) crystallinity.

Table 3
ANOVA for response quadratic model.

Source	df	Sum of square		Mean square		F value		P-value	
		Yield (%)	Crystallinity (%)	Yield (%)	Crystallinity (%)	Yield (%)	Crystallinity (%)	Yield (%)	Crystallinity (%)
Model	9	752.75	788.41	87.61	87.60	249.52	124.75	<0.0001	<0.0001
A	1	9.65	16.56	9.65	16.56	28.81	23.58	0.0030	0.0050
B	1	0.013	9.37	0.01	9.37	0.04	13.35	0.8530	0.0150
C	1	55.17	38.94	55.17	38.94	164.61	55.45	<0.0001	0.0010
AB	1	45.42	212.57	45.42	212.57	135.52	302.73	<0.0001	<0.0001
AC	1	14.02	19.94	14.02	19.94	41.48	28.39	<0.0001	0.0030
BC	1	33.17	27.45	33.17	27.45	98.98	39.10	<0.0001	0.0020
A^2	1	10.92	20.967	33.32	44.19	99.44	62.93	<0.0001	0.0010
B^2	1	161.23	339.09	202.85	366.44	605.17	521.83	<0.0001	<0.0001
C^2	1	423.09	103.51	423.09	103.50	1262.22	147.40	0.0010	<0.0001
Residual error	5	1.67	3.51	0.34	0.702				
Lack of fit	3	0.27	3.50	0.89	1.17	0.13	207.09	0.936	0.005
Pure error	2	1.41	0.011	0.70	0.006				
R^2		0.9978	0.9956						
Adj R^2		0.9938	0.9876						

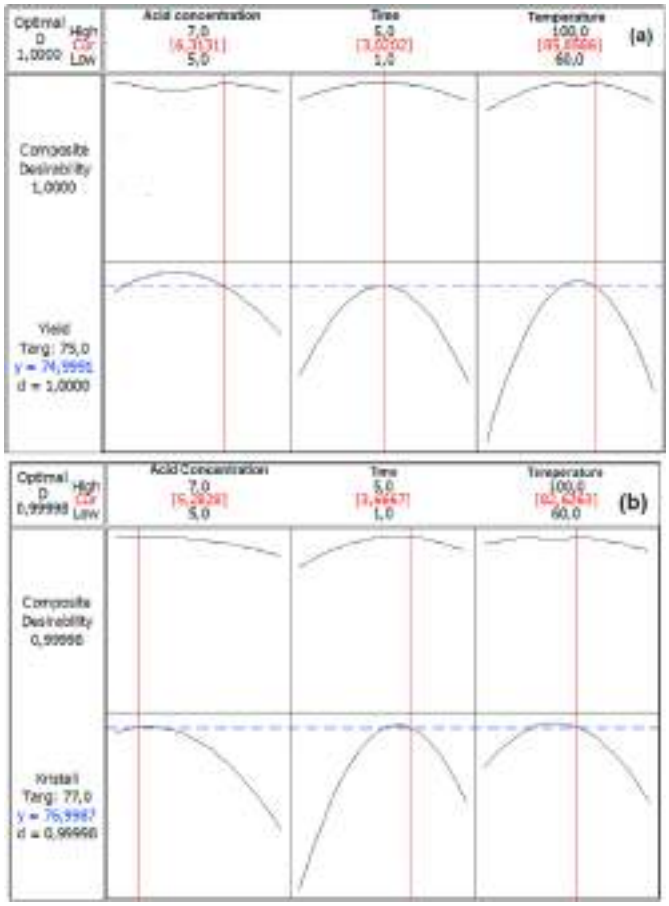

Fig. 6. The curve of optimization results in the yield response (a) and crystallinity (b) of PW-NCLA.

Table 4
Validation of optimization result.

Optimization	Validation result	
	Yield (%)	Crystallinity (%)
Based on yield[a]	75.50	76.69
Based on crystallinity[b]	72.96	75.45

[a] Concentration of acid: 6.31 M, hydrolysis time: 3.02 h, and temperature: 85.86 °C.
[b] Concentration of acid: 5.28 M, hydrolysis time: 3.66 h, and temperature: 82.62 °C.

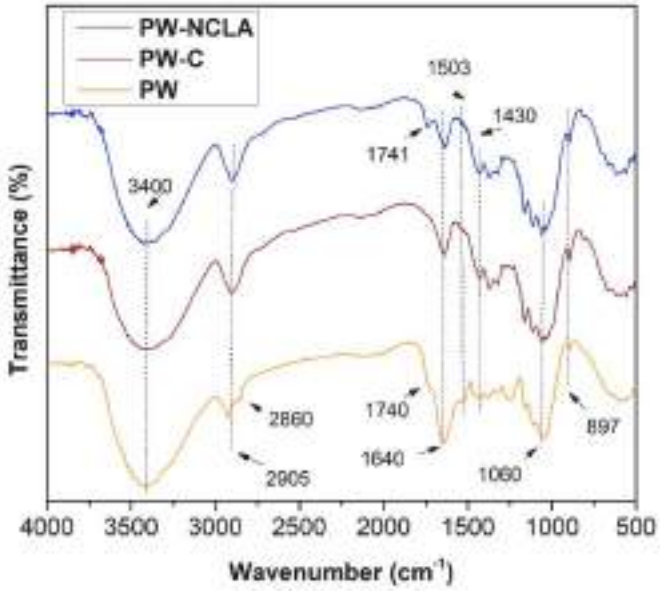

Fig. 7. FTIR spectra of cellulose isolated from PW and PW-NCLA.

optimal conditions for the acid hydrolysis were used to verify the optimization results in Table 4. At optimum hydrolysis conditions, the NCs yield was obtained at 73.45 %, and the crystallinity index was determined at 76.69 %, respectively (Table 4).

3.2. Characterization of nanocellulose

3.2.1. FTIR analysis

FTIR spectra of PW, cellulose and PW-NCLA produced at the optimum condition are shown in Fig. 7. The main absorption bands at 897, 1060, 1430, 1640 and 2905, and 3400 cm^{-1} were observed on lignocellulosic pepper, cellulose, and nanocellulose isolated from the waste. The presence of lignin in lignocellulosic pepper waste (PW) was observed at 1503 cm^{-1}, assigned to the aromatic C═C stretching from the lignin aromatic ring [43]. The carbonyl groups of uronic acids associated with hemicellulose were observed at ~1740 cm^{-1} on pepper waste. The waste also showed the band at 2860 cm^{-1} ascribed to the stretching vibration of the CH_2 group of hemicellulose [26]. The C═O and CH_2 bands of hemicellulose disappeared in PW-C and PW-NCLA; meanwhile, there was no significant difference in the FTIR spectra of

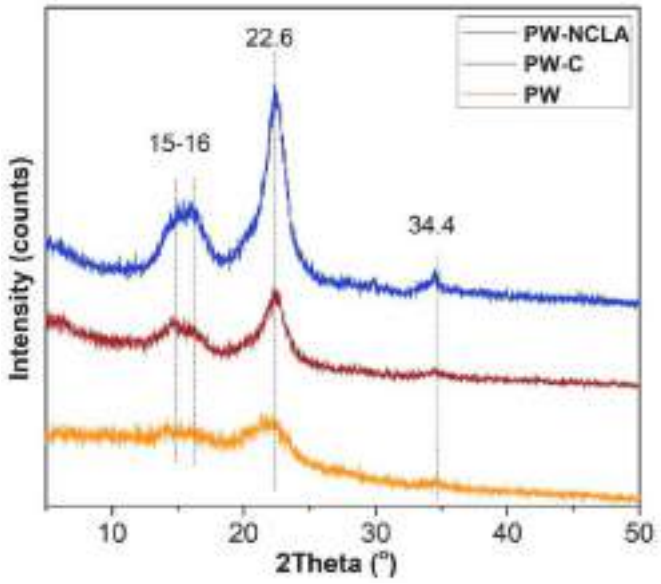

Fig. 8. XRD pattern of cellulose isolated from PW and PW-NCLA.

nanocellulose hydrolyzed using lactic acid with the cellulose.

A band at 1741 cm^{-1} was observed on the spectrum of PW-NCLA, which was assigned to the C═O stretching vibration of adsorbed acetate ion, presumably in the form of cellulose lactate. Lactic acid reacted with the nanocellulose during acid hydrolysis to produce ester groups [16]. Meanwhile, the carboxylic group on the nanocellulose's surface was also released [12]. The absorption band at 897 cm^{-1} indicates the β-glycosidic linkage of the cellulose monomer [44]. The methoxy group of β-1,4-glycosidic linkages was observed at 1060 cm^{-1}. The band at 1430 cm^{-1} indicates the vibrations of cellulose bonds related to crystalline stability. The band at 1640 cm^{-1} was ascribed to O–H bonds bending vibration, while the band at 3400 cm^{-1} is assigned to the O–H stretching vibrations arising from intra and intermolecular hydrogen bonding. Moreover, the band at 2905 cm^{-1} related to the characteristic C–H stretching vibration.

3.2.2. XRD analysis

The XRD analysis of lignocellulosic pepper waste (PW), the isolated cellulose (PW–C), and the hydrolyzed nanocellulose (PW-NCLA) are shown in Fig. 8. PW showed a broad XRD peak centered at 22°, indicating the amorphous structure of lignocellulosic waste [45,46]. Cellulose isolated from PW following alkalization and bleaching treatments slightly increased the crystallinity peak due to removing lignin and hemicellulose. NCs obtained after hydrolysis at optimum conditions demonstrate a higher crystalline peak due to amorphous cellulose removal and high-ordered crystalline structure formation. The XRD data for all samples indicated the main peak at 22.6° ascribed to the cellulose type I, and the amorphous characteristic characterized by a low diffraction intensity at 2θ around 16° [47]. The crystallinity determined according to the [47] method indicates 43.32 % crystallinity for lignocellulosic pepper waste, which enhanced to 56.41 % on PW-C and 72.02 % on PW-NCLA.

The crystallinity index of nanocrystalline cellulose after hydrolysis using lactic acid is approximately similar to our previously reported NCs from oxalic acid and citric acid, at 77.8 % and 76.4 % [7]. Dominic et al. [14] reported using oxalic acid for hydrolysis of rice husk cellulose into NCs and produced nanocrystalline cellulose with crystallinity almost the same PW-NCLA, at 74 %. Nanocrystalline cellulose from corncob waste which was hydrolyzed using organic acids, had a lower crystallinity than PW-NCLA, approximately 63.8 %. The PW-NCLA sample retains the typical crystal pattern of type I cellulose after hydrolysis and ultrasonication.

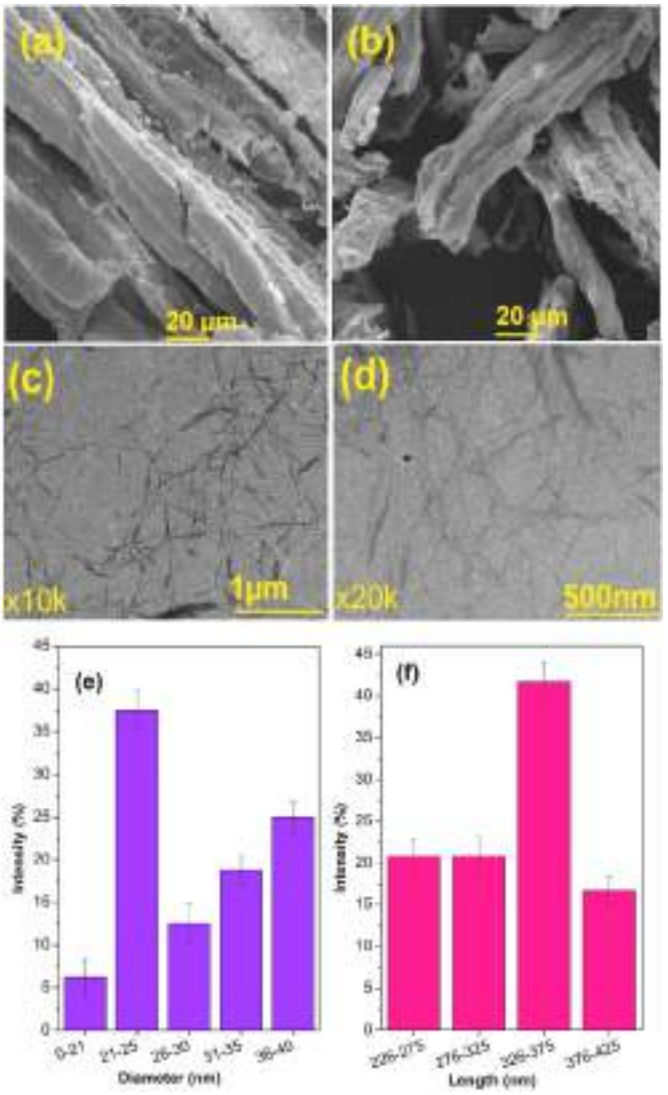

Fig. 9. SEM of industrial pepper waste (PW), cellulose of PW (b), TEM of PW-NCLA with magnification 10 k (c) and 20 k (d), diameter (e), and length (f) distribution of PW-NCLA.

3.2.3. Morphological and particle size analysis

The morphology analysis of pepper waste, cellulose, and nanocrystalline cellulose hydrolyzed using lactic acid at optimized conditions was characterized using SEM and TEM (Fig. 9). SEM analysis of the PW showed a stem-like structure (Fig. 9a). The cellulose isolated from pepper waste appeared smaller in dimension with a more corrugated texture (Fig. 9b). Hydrolysis transformed the cellulose into a uniform nanostructure with a thin rod-shaped morphology (Fig. 9c and d). The diameter of nanocrystalline celluloses was determined at 29.65 ± 3 nm, significantly smaller than the cellulose (Fig. 9e). The length of NCs was measured at 335.19 ± 10 nm. Some nanocellulose from agricultural wastes such as tea stalks, bagasse, corn cobs, and rice husks also have a stem-like structure with diameters of <50 nm [39,48,49].

3.2.4. Particle size and zeta potential analysis

The particle size distribution of dispersed NCs in water was determined using the DLS technique. Fig. 10 shows that the PW-NCLA samples have a narrow distribution, with particle sizes determined in the 100–120 nm range to give an average size of 109 ± 0.6 nm. The zeta potential value is another important indicator for the stability of nanocellulose suspension, which relates to its surface charge. Pepper waste nanocellulose isolated from lactic acid (PW-NCLA) has −26.5 ± 1.6 mV,

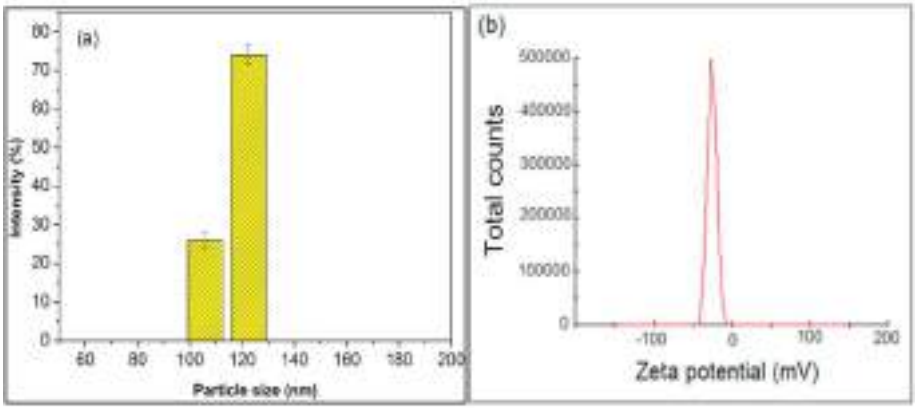

Fig. 10. Overall particle size (a) and zeta potential distributions of PW-NCLA.

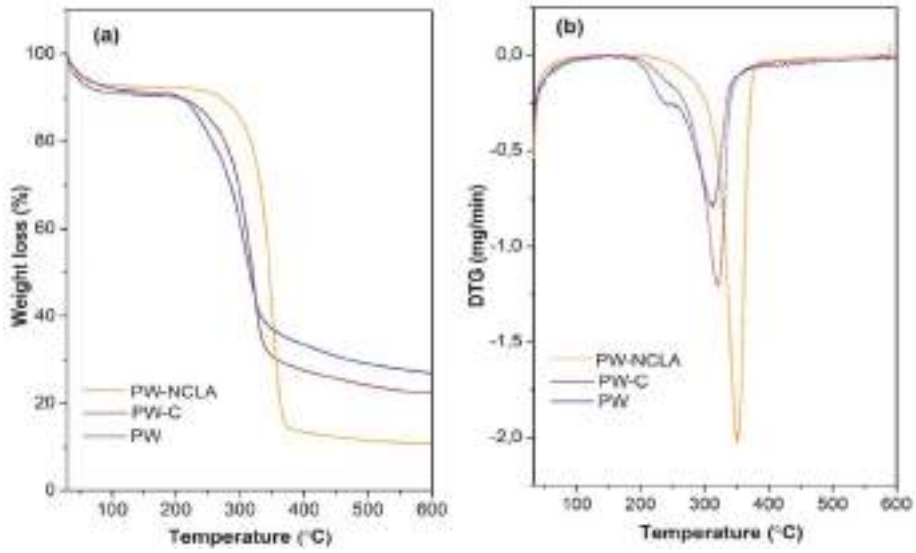

Fig. 11. TGA-DTG curve of waste (PW), cellulose of PW (PW–C), and PW-NCLA.

which indicates good colloidal stability of the nanocelluloses. Natural cellulose fibers contain carboxyl and hydroxyl groups responsible for the negatively charged surfaces [50]. The large surface area in NCs exposes these anionic groups, thus enhancing the negative surface charge.

The residual anionic salt from acid that interacted with the hydroxyl group in cellulose may also affect the zeta potential [16]. NCs obtained from inorganic acid hydrolysis, such as H_2SO_4, showed sulfate anion on the surface, responsible for a high zeta potential value of $\sim -37.9 \pm 2.4$ mV [7]. NCs hydrolyzed with organic acids such as oxalic and citric acid have zeta potential values of −28.0 mV to −28.3 mV, respectively [7], comparable to the NCs obtained using lactic acid in this study. The esterification during hydrolysis between the hydroxyl group and the lactate ion prevents the aggregation of NCs through electrostatic repulsion. Upon submersion in water, the well-dispersed NCs expose the carboxyl and hydroxyl groups for highly negative zeta potential. The formation of NCs with small particle size and high zeta potential indicates the stability of NCs in aqueous suspension, which is perfect as a reinforcement agent for bio-composite polymer [12]. Agglomeration in a nanocellulose suspension occurs when the zeta potential reaches a minimum value of −15 mV [51]. A higher negative zeta potential prevents particle aggregation from the attraction between particles by enhancing electrostatic repulsion [52,53].

Table 5
Thermal properties of PW, PW-C, and PW-NCLA.

Sample	T_o	T_p	$W_{residue}$ (%)
PW	235.8	313.7	27.1
PW-C	269.1	328.7	22.4
PW-NCLA	277.1	350.6	10.8

3.2.5. *Thermal analysis*

Thermal analysis indicates the stability of NCs to endure heat and maintain its mechanical characteristics under extreme conditions. Stability at high temperatures is essential for biomaterial applications [54]. Fig. 11 shows the TG-DTG analysis of pepper waste, cellulose, and nanocellulose, PW-NCLA. PW undergoes three stages of degradation. The first degradation at ~100 °C involved water evacuation from the surface [16]. The second degradation stage at 241 °C indicates the degradation of hemicellulose, which has lower thermal stability than cellulose. Finally, the weight loss at 290–300 °C was due to the decomposition of cellulose.

In contrast to the PW waste powder, cellulose and NCs undergo two stages of decomposition with the absence of degradation at ~240 °C. The weight loss at ~100 °C indicated water desorption on the sample surface, followed by cellulose decomposition at 320–350 °C and [34]. The absence of a peak at 240 °C suggests the absence of hemicellulose in

Table 6
Mechanical properties of bio-composite with seaweed matrix.

Sample	Tensile Strength (MPa)	Elongation at break (%)
Se	37.3 ± 0.3	27.0 ± 0.5
Se–1NC	48.7 ± 0.1	20.7 ± 0.2
Se–3NC	52.8 ± 0.3	18.8 ± 0.6
Se–5NC	56.3 ± 0.3	16.8 ± 0.5
Se–7NC	45.4 ± 0.6	15.9 ± 0.3

cellulose and nanocrystalline cellulose. The temperature for thermal degradation and the weight loss data in Table 5 revealed that NC-LA thermal stability was higher than PW and PW-C. The maximum temperature of NC-LA was observed at 350.60 °C, significantly shifting to a higher temperature due to the high crystallinity of cellulose. The results indicate that hydrolysis using lactic acid successfully removed amorphous cellulose and residual lignin in the cellulose. The residual content of NC-LA following thermal degradation at 600 °C was measured at 10.80 %. The presence of a small amount of carbon residue indicates a high purity of cellulose [55,56]. The degradation temperature at 350.6 °C for NC-LA was comparable with nanocellulose obtained from the hydrolysis of pepper waste using oxalic, citric, and lactic acids but higher than inorganic acids [7]. This is due to the particle size of NCs hydrolyzed using organic acids were larger than inorganic acids, which causes higher thermal stability. Large crystalline cellulose with tightly packed structure has low surface area that is stable towards thermal decomposition [57]. The high crystallinity also inhibits partial disruption of cellulose crystal structure that can reduce the thermal stability of nanocellulose [16].

3.3. Bio-composite properties

3.3.1. Mechanical test

Mechanical tests evaluate the tensile strength and elongation at break of the bio-composite film with 1, 3, 5 and 7 % of PW-NCLA (Table 6). Tensile strength measures the maximum strength when the film is stressed. The tensile strength of biofilm increased from 37.3 ± 0.3 MPa to 48.7 ± 0.1 MPa at 1 wt% PW-NCLA and 56.3 ± 0.3 MPa at 5 % PW-NCLA. The tensile strength was decreased to 45.4 ± 0.6 when 7 % of NCs was added to the biofilm. High surface area of NCs formed strong interfacial interactions via hydrogen or ionic bonds with the polymer matrix. However, the NCs were aggregated at high loading, reducing dispersion in the polymer matrix. Poor dispersion caused non-uniform stress distribution in the film, thereby reducing the strength of the composite film [58]. The results of the tensile test showed that there was an optimum concentration of filler to induce a maximum increase in the

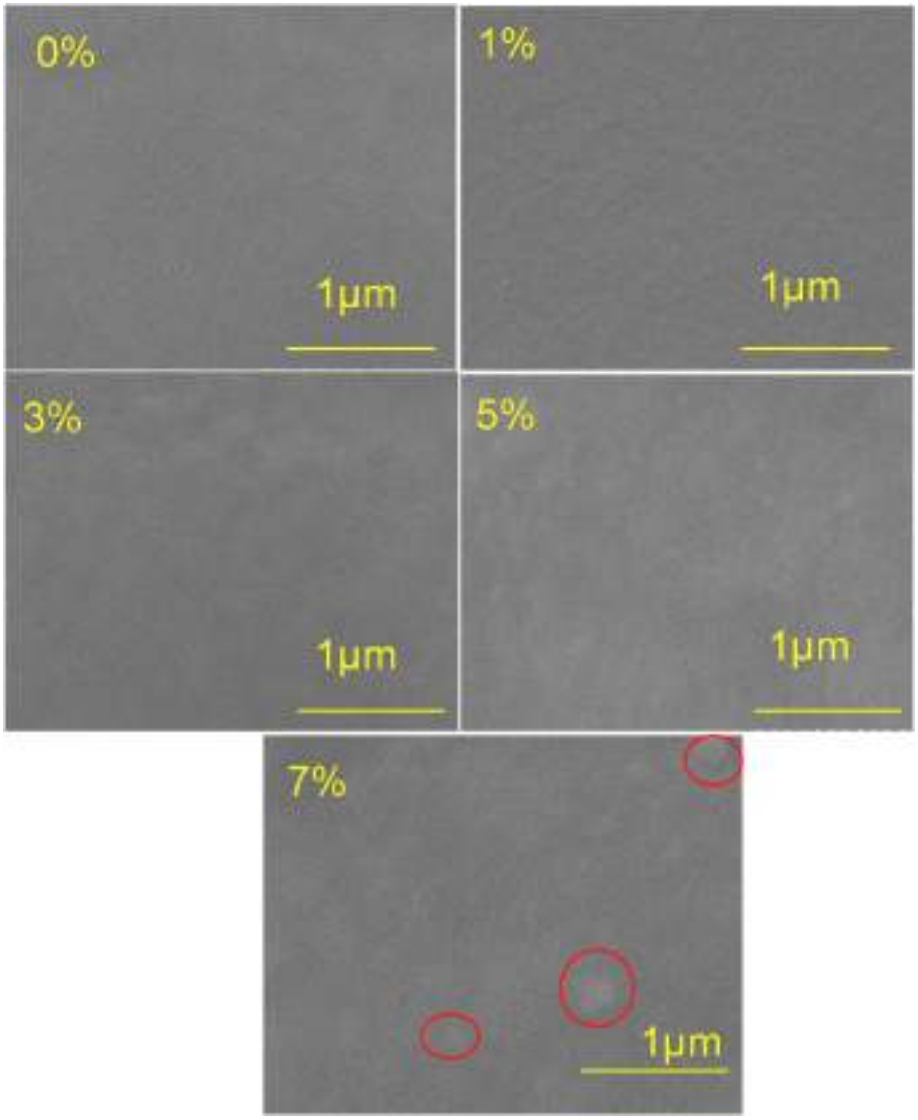

Fig. 12. SEM image of surface of seaweed bio-composite filled with 0, 1, 3, 5 and 7 % of NC-PW.

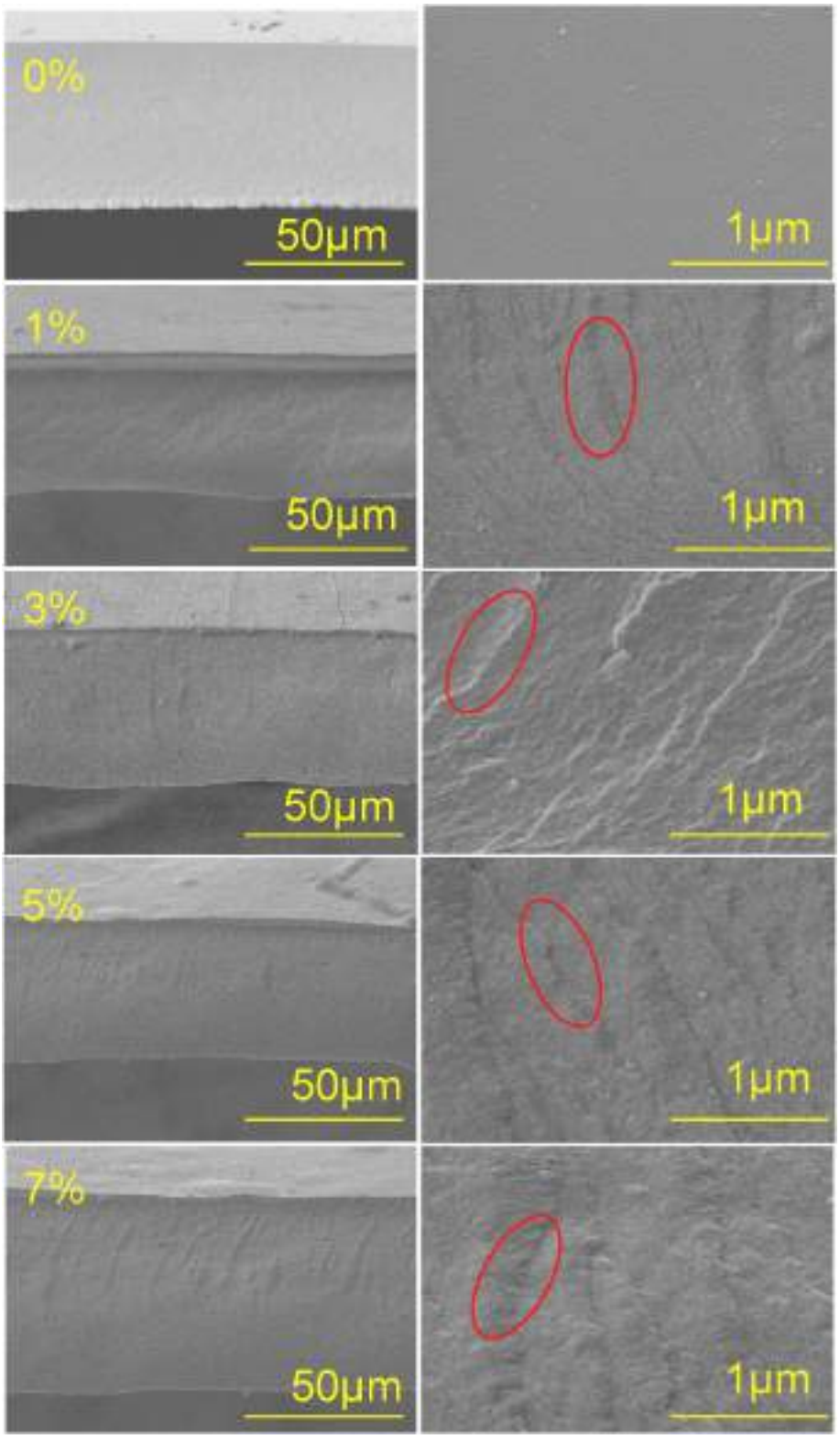

Fig. 13. SEM image of cross section of seaweed bio-composite filled with 0, 1, 3, 5 and 7 % of PW-NCLA.

strength of the composite film.

Elongation at break relates to the extensibility and flexibility of biofilm, which is expressed as a percentage of elongation or strain of the initial film length. Increasing the amount of NCs in biofilm reduced the elongation at break (Table 6). The pure seaweed biofilm showed the highest percentage of elongation at break, namely 27.0 ± 0.5 % and 24.1 ± 0.3 %, respectively. Elongation at break gradually decreased with increasing nanocellulose content. It is possible that the rigid network formed by the nanocellulose and the matrix limits the movement of the molecular matrix chains and reduces the elongation at break [59]. In addition, increasing the amount of nanofiller will limit the mobility of the matrix chains available for elongation and cause a decrease in the deformability of the interface between the filler and the matrix [60]. [61] reported similar results when alginate was modified

Table 7
Water adsorption ability, solubility, and water vapor permeability of seaweed and chitosan bio-composite.

Sample	Thickness (μm)	Water adsorption (%)	Solubility (%)	Water vapor permeability (x10^{-9} g/ m^2 Pa s)
Se	43.3 ± 0.5	15.3 ± 0.05	37.6 ± 0.03	1.49 ± 0.06
Se–1NC	44.5 ± 0.8	14.6 ± 0.03	34.9 ± 0.03	1.35 ± 0.05
Se–3NC	44.8 ± 0.5	13.3 ± 0.02	32.3 ± 0.04	1.26 ± 0.15
Se–5NC	45.6 ± 0.8	13.4 ± 0.08	30.6 ± 0.05	1.19 ± 0.03
Se–7NC	48.2 ± 0.4	12.9 ± 0.05	29.2 ± 0.03	107 ± 0.08

with 6 % cellulose nanowhisker filler, in which the elongation at break reduced from 21.2 % to 14.9 %.

3.3.2. *Morphological analysis*

The surface morphology and cross-section of the seaweed biofilm with PW-NCLA filler were determined using SEM (Fig. 12). The pure seaweed film shows a smooth and homogeneous surface. The addition of nanocellulose up to 5 % shows that the NC particles were well distributed and embedded in the bio-composite matrix. However, the surface became less homogeneous when the PW-NCLA concentration increased to 7 %, indicating the aggregation of nanocellulose in the seaweed matrix [62]. Nevertheless, at low NCs loading, the nanocellulose is well dispersed in the seaweed matrix to form a strong interaction (red circle in Fig. 12). The cross-section of the biofilm was analyzed to determine the miscibility of the NCs in the biofilm (Fig. 13). The nanocellulose is homogenously distributed in the matrix, as indicated by the red circles in the SEM images. However, the cross-section of the seaweed biofilm appears much smoother than the seaweed/NC biofilm. The homogeneous dispersion of nanocellulose implies the compatibility between the PW-NCLA and the matrix via hydrogen bond formation. Similar results have been reported on nanocellulose and starch bio-composite that formed highly cohesively film as characterized by the analysis of cross-sectioned film [63]. Controlling the amount of nanocellulose is essential to achieve high dispersion in the bio-composite and prevent agglomeration [64].

3.3.3. *Water adsorption ability, solubility, and water vapor permeability*

Water adsorption, solubility and water vapor permeability of the biofilm are presented in Table 7. The water content of the Se/NC biofilm at 1–7% nanofiller concentration was 12.9 ± 0.05 % to 14.6 ± 0.03 %, slightly lower than the seaweed biofilm at 15.3 ± 0.5 %. The bio-composite also showed a significant decrease in moisture content when the PW-NCLA concentration increased from 1 % to 7 % (w/w). The hydrophilicity of bio-composite film is reduced by adding nanocellulose due to strong hydrogen bonds between the nanofiller/matrix, thereby limiting water interaction. The solubility of film in water determines the potential application in food packaging to ensure food safety. The application of seaweed in food packaging is still limited because of its rapid water absorption. Therefore, adding nanocellulose filler to the seaweed matrix is expected to overcome this limitation. Based on observation, the seaweed bio-composite disintegrated when submerged in water. Nevertheless, the addition of PW-NCLA reduced the solubility of the film from 37.6 ± 0.03 % to 29.2 ± 0.03 at 7 % of nanocellulose.

Nanocellulose interacts with the seaweed matrix via hydrogen bond formation, consequently increasing water resistance and stability of the seaweed/NC films. The interfacial interaction increased the cohesive properties and reduced water sensitivity since water molecules cannot dissociate the strong hydrogen bonds in bio-composite [65]. Ilyas et al. [63] and Lu et al. [66] reported that the resulting matrix structure between filler/filler and matrix/filler interactions is a relevant aspect for identifying the strengthening effect of nanofiller. The hydroxyl groups in the NCs formed strong interfacial interactions through hydrogen bonds with the polymer matrix, reducing the freely available hydroxyl group [31]. The hydrogen bond reduced hydrophilicity, water permeability and solubility of bio-composites [32–35]. It can be concluded that the addition of NC nanofiller can increase the water resistance properties of the film, which is an important characteristic in food packaging and can increase the shelf life of food products.

Water vapor permeability measures the water vapor transmission rate through the material. Biofilm with low water vapor permeability prevents moisture transfer from the environment. Therefore, minimizing water permeability is essential for application in food packaging. Nanocellulose improves the water vapor barrier in biofilm by providing rigid crystalline regions to restrict gas diffusion. The water vapor permeability decreases from 1.49 ± 0.06 × 10^{-9} g/m^2 Pa s for the seaweed film to 1.07 × 10^{-9} g/m^2 Pa.s at 7 % NCs loading (Table 7). The degree of crystallinity is essential in the permeability behavior of the nanocomposite [67]. Water vapor has higher diffusibility through the amorphous area than the crystalline region of the polymer matrix. NCs increased the tortuosity in biofilm, reducing the permeability for water vapor diffusion [64]. The NCs were also suggested to improve the impermeable barrier against moisture by increasing the diffusion path of water vapor through the film [68].

4. Conclusion

The parameters of lactic acid hydrolysis were optimized using the second-order polynomial model to produce highly crystalline nanocellulose from pepper biowaste. The response of yield and crystallinity were linearly correlated by acid concentration, temperature, and hydrolysis time. Optimized hydrolysis parameters at 85.86 °C and 3.02 h, while using 6.31 M of lactic acid, produced 75.50 % of NCs with 76.69 % of crystallinity index. The NCs have short rod-like structures with a diameter and length of 29.65 ± 3.1 nm and 335.19 ± 10.2 nm, respectively. The NC-LA exhibited high thermal stability at 350.6 °C and a zeta potential of −26.5 ± 1.6 mV. When applied as filler in seaweed, the nanocellulose is well dispersed in the matrix, producing bio-composite film with smooth morphology. The addition of 5 % nanocellulose filler to the seaweed bio-composite film increased the tensile strength to 56.3 ± 0.3 MPa. The water adsorption rate, solubility and water permeability of the NC/seaweed bio-composite decreased as the amount of NCs increased.

Declaration of competing interest

The authors declare that they have no known competing financial interests or personal relationships that could have appeared to influence the work reported in this paper.

Acknowledgment

The authors acknowledge Institut Teknologi Sepuluh Nopember and BRIN Cibinong, Indonesia, under research grants HETI ADB No. 2316/PKS/ITS/2022, RIIM 3 No. 12/III.5/HK/2023 and ORM grant 2022-2023.

References

[1] Brinchi L, Cotana F, Fortunati E, Kenny JM. Production of nanocrystalline cellulose from lignocellulosic biomass: technology and applications. Carbohydr Polym 2013; 94:154–69. https://doi.org/10.1016/j.carbpol.2013.01.033.

[2] Haque A, Mondal D, Khan I, Usmani MA, Bhat AH, Gazal U. Fabrication of composites reinforced with lignocellulosic materials from agricultural biomass. Lignocellulosic fibre and biomass-based composite materials: processing, properties and applications. Elsevier Inc.; 2017. p. 179–91. https://doi.org/10.1016/B978-0-08-100959-8.00010-X.

[3] Lee HV, Hamid SBA, Zain SK. Conversion of lignocellulosic biomass to nanocellulose: structure and chemical process. Sci World J 2014;2014. https://doi.org/10.1155/2014/631013.

[4] Chen L, Abdalkarim SYH, Yu H, Chen X, Tang D, Li Y, et al. Nanocellulose-based functional materials for advanced energy and sensor applications. Nano Res 2022; 15:7432–52. https://doi.org/10.1007/s12274-022-4374-7.

[5] Yu HY, Zhang DZ, Lu FF, Yao J. New approach for single-step extraction of carboxylated cellulose nanocrystals for their use as adsorbents and flocculants. ACS Sustainable Chem Eng 2016;4:2632–43. https://doi.org/10.1021/acssuschemeng.6b00126.

[6] Montero B, Rico M, Rodríguez-Llamazares S, Barral L, Bouza R. Effect of nanocellulose as a filler on biodegradable thermoplastic starch films from tuber, cereal and legume. Carbohydr Polym 2017;157:1094–104. https://doi.org/10.1016/j.carbpol.2016.10.073.

[7] Holilah H, Bahruji H, Ediati R, Asranudin A. Uniform rod and spherical nanocrystalline celluloses from hydrolysis of industrial pepper waste (Piper nigrum L.) using organic acid and inorganic acid. Int J Biol Macromol 2022;204:593–605. https://doi.org/10.1016/j.ijbiomac.2022.02.045.

[8] Mäki-Arvela P, Salmi T, Holmbom B, Willför S, Murzin DY. Synthesis of sugars by hydrolysis of hemicelluloses- A review. Chem Rev 2011;111:5638–66. https://doi.org/10.1021/CR2000042/ASSET/CR2000042.FP.PNG_V03.

[9] Negahdar L, Delidovich I, Palkovits R. Aqueous-phase hydrolysis of cellulose and hemicelluloses over molecular acidic catalysts: insights into the kinetics and reaction mechanism. Appl Catal, B 2016;184:285–98. https://doi.org/10.1016/J.APCATB.2015.11.039.

[10] Ma Y, Xia Q, Liu Y, Chen W, Liu S, Wang Q, et al. Production of nanocellulose using hydrated deep eutectic solvent combined with ultrasonic treatment. ACS Omega 2019;4:8539–47. https://doi.org/10.1021/acsomega.9b00519.

[11] Ramadhani DV, Holilah H, Bahruji H, Jadid N, Oetami TP, Jalil AA, et al. Effect of lignocellulosic composition of Reutealis trisperma waste on nanocrystalline cellulose properties. Biocatal Agric Biotechnol 2022;45:102516. https://doi.org/10.1016/J.BCAB.2022.102516.

[12] Nagarajan KJ, Balaji AN, Kasi Rajan ST, Ramanujam NR. Preparation of bio-eco based cellulose nanomaterials from used disposal paper cups through citric acid hydrolysis. Carbohydr Polym 2020;235. https://doi.org/10.1016/j.carbpol.2020.115997.

[13] Cherian BM, Pothan LA, Nguyen-Chung T, Mennig G, Kottaisamy M, Thomas S. A novel method for the synthesis of cellulose nanofibril whiskers from banana fibers and characterization. J Agric Food Chem 2008;56:5617–27. https://doi.org/10.1021/jf8003674.

[14] Dominic M, Joseph R, Sabura Begum PM, Kanoth BP, Chandra J, Thomas S. Green tire technology: effect of rice husk derived nanocellulose (RHNC) in replacing carbon black (CB) in natural rubber (NR) compounding. Carbohydr Polym 2020; 230:115620. https://doi.org/10.1016/j.carbpol.2019.115620.

[15] Henschen J, Li D, Ek M. Preparation of cellulose nanomaterials via cellulose oxalates. Carbohydr Polym 2019;213:208–16. https://doi.org/10.1016/j.carbpol.2019.02.056.

[16] Liu C, Li B, Du H, Lv D, Zhang Y, Yu G, et al. Properties of nanocellulose isolated from corncob residue using sulfuric acid, formic acid, oxidative and mechanical methods. Carbohydr Polym 2016;151:716–24. https://doi.org/10.1016/J.CARBPOL.2016.06.025.

[17] Poonguzhali R, Khaleel Basha S, Sugantha Kumari V. Synthesis of alginate/nanocellulose bionanocomposite for in vitro delivery of ampicillin. Polym Bull 2018;75:4165–73. https://doi.org/10.1007/s00289-017-2253-2.

[18] Chaisu K, Charles AL, Guu Y-K, Yen T-B, Chiu C-H. Optimization lactic acid production from molasses renewable raw material through response surface methodology with Lactobacillus casei M-15. APCBEE Procedia 2014;8:194–8. https://doi.org/10.1016/j.apcbee.2014.03.026.

[19] Sun B, Peng G, Duan L, Xu A, Li X. Pretreatment by NaOH swelling and then HCl regeneration to enhance the acid hydrolysis of cellulose to glucose. Bioresour Technol 2015;196:454–8. https://doi.org/10.1016/J.BIORTECH.2015.08.009.

[20] Guo Y, Zhang Y, Zheng D, Li M, Yue J. Isolation and characterization of nanocellulose crystals via acid hydrolysis from agricultural waste-tea stalk. Int J Biol Macromol 2020;163:927–33. https://doi.org/10.1016/j.ijbiomac.2020.07.009.

[21] Wijaya CJ, Ismadji S, Aparamarta HW, Gunawan S. Optimization of cellulose nanocrystals from bamboo shoots using Response Surface Methodology. Heliyon 2019;5:e02807. https://doi.org/10.1016/j.heliyon.2019.e02807.

[22] Davoudpour Y, Hossain MS, Abdul Khalil HPS, Mohamad Haafiz MK, Mohd Ishak ZA, Hassan A, et al. Optimization of high pressure homogenization parameters for the isolation of cellulosic nanofibers using response surface methodology. Ind Crops Prod 2015;74:381–7. https://doi.org/10.1016/j.indcrop.2015.05.029.

[23] Ngwabebhoh FA, Erdem A, Yildiz U. A design optimization study on synthesized nanocrystalline cellulose, evaluation and surface modification as a potential biomaterial for prospective biomedical applications. Int J Biol Macromol 2018; 114:536–46. https://doi.org/10.1016/j.ijbiomac.2018.03.155.

[24] Guo Y, Zhang Y, Zheng D, Li M, Yue J. Isolation and characterization of nanocellulose crystals via acid hydrolysis from agricultural waste-tea stalk. Int J Biol Macromol 2020;163:927–33. https://doi.org/10.1016/j.ijbiomac.2020.07.009.

[25] Wijaya CJ, Ismadji S, Aparamarta HW, Gunawan S. Optimization of cellulose nanocrystals from bamboo shoots using Response Surface Methodology. Heliyon 2019;5:e02807. https://doi.org/10.1016/j.heliyon.2019.e02807.

[26] Holilah H, Prasetyoko D, Ediati R, Bahruji H, Jalil AA, Asranudin A, et al. Hydrothermal assisted isolation of microcrystalline cellulose from pepper (Piper nigrum L.) processing waste for making sustainable bio-composite. J Clean Prod 2021;305:127229. https://doi.org/10.1016/j.jclepro.2021.127229.

[27] Dong Y, Xie Y, Ma X, Yan L, Yu HY, Yang M, et al. Multi-functional nanocellulose based nanocomposites for biodegradable food packaging: hybridization, fabrication, key properties and application. Carbohydr Polym 2023:321. https://doi.org/10.1016/j.carbpol.2023.121325.

[28] Liao Y, Wang C, Dong Y, Yu HY. Robust and versatile superhydrophobic cellulose-based composite film with superior UV shielding and heat-barrier performances for sustainable packaging. Int J Biol Macromol 2023:253. https://doi.org/10.1016/j.ijbiomac.2023.127178.

[29] Qin CC, Abdalkarim SYH, Yang MC, Dong YJ, Yu HY, Ge D. All-naturally structured tough, ultrathin, and washable dual-use composite for fruits preservation with high biosafety evaluation. Int J Biol Macromol 2023;247. https://doi.org/10.1016/j.ijbiomac.2023.125828.

[30] Montero B, Rico M, Rodríguez-Llamazares S, Barral L, Bouza R. Effect of nanocellulose as a filler on biodegradable thermoplastic starch films from tuber, cereal and legume. Carbohydr Polym 2017;157:1094–104. https://doi.org/10.1016/j.carbpol.2016.10.073.

[31] Perumal AB, Sellamuthu PS, Nambiar RB, Sadiku ER, Adeyeye OA. Biocomposite reinforced with nanocellulose for packaging applications. Singapore: Springer; 2019. p. 83–123. https://doi.org/10.1007/978-981-13-8063-1_4.

[32] Shankar S, Rhim JW. Preparation of nanocellulose from micro-crystalline cellulose: the effect on the performance and properties of agar-based composite films. Carbohydr Polym 2016;135:18–26. https://doi.org/10.1016/j.carbpol.2015.08.082.

[33] Hasan M, Lai TK, Gopakumar DA, Jawaid M, Owolabi FAT, Mistar EM, et al. Micro crystalline bamboo cellulose based seaweed biodegradable composite films for sustainable packaging. Material. J Polym Environ 2019;27:1602–12. https://doi.org/10.1007/s10924-019-01457-4.

[34] Kumar Rai G, Singh VP. Study of fabrication and analysis of nanocellulose reinforced polymer matrix composites. Mater Today Proc 2020. https://doi.org/10.1016/j.matpr.2020.06.018.

[35] Lee H, You J, Jin HJ, Kwak HW. Chemical and physical reinforcement behavior of dialdehyde nanocellulose in PVA composite film: a comparison of nanofiber and nanocrystal. Carbohydr Polym 2020;232:115771. https://doi.org/10.1016/j.carbpol.2019.115771.

[36] Syafri E, Sudirman, Mashadi, Yulianti E, Deswita, Asrofi M, et al. Effect of sonication time on the thermal stability, moisture absorption, and biodegradation of water hyacinth (Eichhornia crassipes) nanocellulose-filled bengkuang (Pachyrhizus erosus) starch biocomposites. J Mater Res Technol 2019;8:6223–31. https://doi.org/10.1016/j.jmrt.2019.10.016.

[37] Gontard N, Guilbert S, Cuq J-L. Water and glycerol as plasticizers affect mechanical and water vapor barrier properties of an edible wheat gluten film. J Food Sci 1993; 58:206–11. https://doi.org/10.1111/j.1365-2621.1993.tb03246.x.

[38] Nagarajan KJ, Balaji AN, Kasi Rajan ST, Ramanujam NR. Preparation of bio-eco based cellulose nanomaterials from used disposal paper cups through citric acid hydrolysis. Carbohydr Polym 2020;235:115997. https://doi.org/10.1016/j.carbpol.2020.115997.

[39] Guo Y, Zhang Y, Zheng D, Li M, Yue J. Isolation and characterization of nanocellulose crystals via acid hydrolysis from agricultural waste-tea stalk. Int J Biol Macromol 2020;163:927–33. https://doi.org/10.1016/j.ijbiomac.2020.07.009.

[40] Sun B, Yu HY, Zhou Y, Huang Z, Yao JM. Single-step extraction of functionalized cellulose nanocrystal and polyvinyl chloride from industrial wallpaper wastes. Ind Crops Prod 2016;89:66–77. https://doi.org/10.1016/j.indcrop.2016.04.040.

[41] Ye S, Yu HY, Wang D, Zhu J, Gu J. Green acid-free one-step hydrothermal ammonium persulfate oxidation of viscose fiber wastes to obtain carboxylated spherical cellulose nanocrystals for oil/water Pickering emulsion. Cellulose 2018; 25:5139–55. https://doi.org/10.1007/s10570-018-1917-x.

[42] Koocheki A, Taherian AR, Razavi SMA, Bostan A. Response surface methodology for optimization of extraction yield, viscosity, hue and emulsion stability of mucilage extracted from Lepidium perfoliatum seeds. Food Hydrocolloids 2009;23: 2369–79. https://doi.org/10.1016/J.FOODHYD.2009.06.014.

[43] Sheltami RM, Abdullah I, Ahmad I, Dufresne A, Kargarzadeh H. Extraction of cellulose nanocrystals from mengkuang leaves (Pandanus tectorius). Carbohydr Polym 2012;88:772–9. https://doi.org/10.1016/j.carbpol.2012.01.062.

[44] Naduparambath S TVJ, Shaniba V MPS, Balan AK, Purushothaman E. Isolation and characterisation of cellulose nanocrystals from sago seed shells. Carbohydr Polym 2018;180:13–20. https://doi.org/10.1016/j.carbpol.2017.09.088.

[45] Duchemin B, Thuault A, Vicente A, Rigaud B, Fernandez C, Eve S. Ultrastructure of cellulose crystallites in flax textile fibres. Cellulose 2012;19:1837–54. https://doi.org/10.1007/s10570-012-9786-1.

[46] Owolabi AF, Haafiz MKM, Hossain MS, Hussin MH, Fazita MRN. Influence of alkaline hydrogen peroxide pre-hydrolysis on the isolation of microcrystalline cellulose from oil palm fronds. Int J Biol Macromol 2017;95:1228–34. https://doi.org/10.1016/j.ijbiomac.2016.11.016.

[47] Segal L, Creely JJ, Martin AE, Conrad CM. An empirical method for estimating the degree of crystallinity of native cellulose using the X-ray diffractometer. Textil Res J 1959;29:786–94. https://doi.org/10.1177/004051755902901003.

[48] Mandal S, Chatterjee B, Layek B. Cellulose-based nanomaterials in drug delivery applications. Biopolymer-based nanomaterials in drug delivery and biomedical applications. Elsevier; 2021. p. 57–86. https://doi.org/10.1016/b978-0-12-820874-8.00003-8.

[49] Rashid S, Dutta H. Characterization of nanocellulose extracted from short, medium and long grain rice husks. Ind Crops Prod 2020;154:112627. https://doi.org/10.1016/j.indcrop.2020.112627.

[50] Stana-Kleinschek K, Ribitsch V. Electrokinetic properties of processed cellulose fibers. Colloids Surf A Physicochem Eng Asp 1998;140:127–38. https://doi.org/10.1016/S0927-7757(97)00301-4.
[51] Faradilla RHF, Lee G, Arns JY, Roberts J, Martens P, Stenzel MH, et al. Characteristics of a free-standing film from banana pseudostem nanocellulose generated from TEMPO-mediated oxidation. Carbohydr Polym 2017;174:1156–63. https://doi.org/10.1016/j.carbpol.2017.07.025.
[52] Prathapan R, Thapa R, Garnier G, Tabor RF. Modulating the zeta potential of cellulose nanocrystals using salts and surfactants. Colloids Surf A Physicochem Eng Asp 2016;509:11–8. https://doi.org/10.1016/j.colsurfa.2016.08.075.
[53] Whba F, Mohamed F, Idris MI, Yahya MS. Surface modification of cellulose nanocrystals (CNCs) to form a biocompatible, stable, and hydrophilic substrate for MRI. Appl Sci 2023;13. https://doi.org/10.3390/app13106316.
[54] Ilyas RA, Sapuan SM, Ishak MR, Zainudin ES. Sugar palm nanofibrillated cellulose (Arenga pinnata (Wurmb.) Merr): effect of cycles on their yield, physic-chemical, morphological and thermal behavior. Int J Biol Macromol 2019;123:379–88. https://doi.org/10.1016/J.IJBIOMAC.2018.11.124.
[55] Fardioui M, Stambouli A, Gueddira T, Dahrouch A, Qaiss AEK, Bouhfid R. Extraction and characterization of nanocrystalline cellulose from doum (chamaerops humilis) leaves: a potential reinforcing biomaterial. J Polym Environ 2016;24:356–62. https://doi.org/10.1007/s10924-016-0784-5.
[56] Tarchoun AF, Trache D, Klapötke TM. Microcrystalline cellulose from Posidonia oceanica brown algae: extraction and characterization. Int J Biol Macromol 2019;138:837–45. https://doi.org/10.1016/j.ijbiomac.2019.07.176.
[57] Rafeny NHB, Bahruji H, Abdullah R, Mahadi AH, Prasetyoko D. Subcritical water hydrolysis of cotton fibers to nanocellulose for producing poly(vinyl alcohol)/cellulose biocomposite. Starch - Stärke 2023;75:2300065. https://doi.org/10.1002/STAR.202300065.
[58] Reddy JP, Rhim JW. Characterization of bionanocomposite films prepared with agar and paper-mulberry pulp nanocellulose. Carbohydr Polym 2014;110:480–8. https://doi.org/10.1016/j.carbpol.2014.04.056.
[59] Chen Q, Liu Y, Chen G. A comparative study on the starch-based biocomposite films reinforced by nanocellulose prepared from different non-wood fibers. Cellulose 2019;26:2425–35. https://doi.org/10.1007/s10570-019-02254-x.
[60] Abdul Khalil HPS, Tye YY, Ismail Z, Leong JY, Saurabh CK, Lai TK, et al. Oil palm shell nanofiller in seaweed-based composite film: mechanical, physical, and morphological properties. Bioresources 2017;12:5996–6010. https://doi.org/10.15376/biores.12.3.5996-6010.
[61] Wang LF, Shankar S, Rhim JW. Properties of alginate-based films reinforced with cellulose fibers and cellulose nanowhiskers isolated from mulberry pulp. Food Hydrocolloids 2017;63:201–8. https://doi.org/10.1016/j.foodhyd.2016.08.041.
[62] Agustin MB, Ahmmad B, De Leon ERP, Buenaobra JL, Salazar JR, Hirose F. Starch-based biocomposite films reinforced with cellulose nanocrystals from garlic stalks. Polym Compos 2013;34:1325–32. https://doi.org/10.1002/pc.22546.
[63] Ilyas RA, Sapuan SM, Ishak MR. Isolation and characterization of nanocrystalline cellulose from sugar palm fibres (Arenga Pinnata). Carbohydr Polym 2018;181:1038–51. https://doi.org/10.1016/j.carbpol.2017.11.045.
[64] Khan A, Khan RA, Salmieri S, Le Tien C, Riedl B, Bouchard J, et al. Mechanical and barrier properties of nanocrystalline cellulose reinforced chitosan based nanocomposite films. Carbohydr Polym 2012;90:1601–8. https://doi.org/10.1016/j.carbpol.2012.07.037.
[65] Tunc S, Angellier H, Cahyana Y, Chalier P, Gontard N, Gastaldi E. Functional properties of wheat gluten/montmorillonite nanocomposite films processed by casting. J Membr Sci 2007;289:159–68. https://doi.org/10.1016/J.MEMSCI.2006.11.050.
[66] Lu Y, Weng L, Cao X. Biocomposites of plasticized starch reinforced with cellulose crystallites from cottonseed linter. Macromol Biosci 2005;5:1101–7. https://doi.org/10.1002/mabi.200500094.
[67] Rhim JW, Park HM, Ha CS. Bio-nanocomposites for food packaging applications. Prog Polym Sci 2013;38:1629–52. https://doi.org/10.1016/j.progpolymsci.2013.05.008.
[68] Su JF, Huang Z, Yuan XY, Wang XY, Li M. Structure and properties of carboxymethyl cellulose/soy protein isolate blend edible films crosslinked by Maillard reactions. Carbohydr Polym 2010;79:145–53. https://doi.org/10.1016/j.carbpol.2009.07.035.